TRANSACTIONS OF THE INSTITUTE OF MEASUREMENT & CONTROL

Transactions of the Institute of Measurement and Control
1–14

DOI: 10.1177/01423312221100340
journals.sagepub.com/home/tim
SAGE

Unmanned aerial vehicle formation obstacle avoidance control based on light transmission model and improved artificial potential field

Jiacheng Li[1], Yangwang Fang[1], Haoyu Cheng[1], Zhikai Wang[2] and Shuaiqi Huangfu[1]

Abstract

To overcome the limitations of the conventional artificial potential field (APF) method, which is commonly used for unmanned aerial vehicle (UAV) formation obstacle avoidance control. A novel UAV formation obstacle avoidance control method based on a light transmission model (LTM) and an improved APF method is proposed. First, inspired by the flight of bird flocks, we combine the LTM with an APF function to present an improved APF model which can help UAV find feasible free space to maneuver. From this, UAV can overcome the drawbacks of non-reachable and local minima under the action of LTM. Then, the obstacle avoidance strategy based on the fixed-wing UAV motion model is proposed, and the obstacle avoidance control algorithm for UAV formation is designed. Finally, simulation results show the effectiveness and superiority of the proposed method, which can result in a dramatic improvement in the performance of UAV formation to obstacle avoidance under the complex and non-deterministic environment.

Keywords

Unmanned aerial vehicle, improved artificial potential field, obstacle avoidance, formation, light transmission model

Introduction

Currently, with the continuous advancement of communication technology, the trend of completing tasks of civilian and military via unmanned aerial vehicle (UAV) formation is growing year by year (Ali and Zhangang, 2021; Chang et al., 2020; Hu et al., 2020), where the obstacle avoidance ability of formation is a key to flying. Studying the obstacle avoidance control of formation can improve the coordination, intelligence, and autonomy of UAV, which can improve the operational efficiency of UAV formation in military fields such as coordinated search, electronic countermeasures, and cluster attacks. At the same time, UAV formation with obstacle avoidance function can adapt to various and complex flight environments, which have good application prospects in civilian fields such as plant protection, power inspection, security, and logistics. However, obstacle avoidance for UAV formation under uncertain and complex flying environments is still a challenge so far (Singla et al., 2021; Sui et al., 2021; Yan et al., 2021; Yang et al., 2021).

At present, obstacle avoidance algorithms by mathematical planning, graph theory, spatial decomposition, intelligent algorithm, random planning, machine learning, and potential field are several common ways that have proven to be effective (Fu et al., 2020; Hu et al., 2020; Huang et al., 2019; Liu et al., 2019; Wu et al., 2020). Of course, in the actual obstacle avoidance process, a mixture of one or more of the above obstacle avoidance methods is usually used. Because the artificial potential field (APF) method has some advantages of high flexibility, simple calculation, and powerful real-time, it is widely used in obstacle avoidance. The principles of the APF method are setting the target point with attraction and the obstacles with repulsion to UAV artificially, which can realize the obstacle avoidance and navigation of formation. However, the main shortages of the artificial field method are existed the non-reachable point and local minima area (Li et al., 2020; Lin et al., 2021; Pan et al., 2021).

There has been considerable recent research in the area of improving the APF method which can be classified into two major categories (Hu et al., 2020; Mancini et al., 2020; Wu et al., 2021; Zappulla et al., 2019). One is to improve the APF method based on itself. For instance, Yun and Tan (1997) proposed a wall-following algorithm when the robots are placed in a local minimum. Besides, some scholars also added a new force into UAVs for escaping local minima in potential

[1]Unmanned System Research Institute, Northwestern Polytechnical University, P.R. China
[2]School of Aeronautics, Northwestern Polytechnical University, P.R. China

Corresponding author:
Yangwang Fang, Unmanned System Research Institute, Northwestern Polytechnical University, 127 West Youyi Road, Beilin District, Xi'an 710072, Shaanxi, P.R. China.
Email: ywfang@nwpu.edu.cn

fields. Such as, a new repulsion field whose directional coordination force is coupled with the relative distance between the UAV and the target was constructed in Chen et al. (2018). Wang et al. (2020) used a collision prediction model (CPM) with APF to overcome the dynamic obstacle environment, which is similar to Song et al. (2020) that resolved the local minimum through a predictive APF. Lee et al. (2018) helped the mobile robot to overcome local minima and path inefficiency drawbacks via a new point of attractive force. Moreover, with reference to the methodology from machine learning, a decision tree was introduced in Lin et al. (2020) to improve the dynamic path planning problem of robots in an indoor complex environment. Another is to solve the local minima problem using the method of combining the APF method with intelligence algorithm. For example, Orozco-Rosas et al. (2019) mentioned an approach to seek a feasible and safe path with combined membrane computing, genetic algorithm, and APF. A mixture of approaches including probabilistic roadmap (PRM), A* heuristic, and particle swarm optimization (PSO) algorithm was proposed in Raheem and Abdulkareem (2020). Cahyadi et al. (2020) improved APF with the combination of power diagram optimization strategy. Furthermore, Wang et al. (2020) combined fuzzy APF with an extensible neural network algorithm, which can guide the robots to move with a better path planning in complex dynamic environment.

Besides, a novel distributed and priority-based platform of guidance and control model was proposed in Haghighi et al. (2019), which can meet requirements for each UAV coordinated maneuver. In the same time, the proposed algorithm provides outstanding following performance and inherent collision avoidance pattern due to prioritized tracking. Haghighi et al. (2021) proposed a new efficient modified A* algorithm with a novel defined criterion based on the three-dimensional mountainous environment, which can solve the cooperated multi-agent patrolling with online mapping and dynamic situation of cooperated agents. However, as the number of UAVs in the formation increases, the information that needs to be coordinated between UAVs in Haghighi et al. (2021) will increase, which seems to affect the computational complexity of the algorithm. A novel control function was proposed in Park and Yoo (2021) for a robust leader–follower formation tracking, which can guarantee the connectivity between the leader and the followers in the case of avoiding an obstacle. It is beneficial to the practical control application of multi-agent coordination obstacle avoidance. The problem of collision avoidance and obstacle avoidance for multiple UAVs can be solved via a novel distributed cooperative control algorithm proposed in Qi et al. (2022), in which repulsion function is based on Hooke's law and can calculate the optimal velocity to keep the UAVs away from obstacles in the field of view. However, the control effect of this method has high uncertainty when under the denied environment.

The common limitations of these collision avoidance strategies are that they are only suitable for a single UAV in collision avoidance, but not applicable to a formation of UAVs. And some of these methods are suitable for formation collision avoidance, but have limitations of expensive computing cost, long time for iterative optimization, and difficulty of dealing with uncertain and complex environments. Here, an environment that has dense, randomly arranged, irregular obstacles or groups of obstacles can be considered as complex.

Based on the above discussion, a UAV formation obstacle avoidance control method is proposed in this paper. Compared to the existing literature, this paper offers the following contributions:

1. We provide an improved APF method based on the light transmission model (LTM) to ensure UAVs finding feasible free space to maneuver, which can eliminate the non-reachable and local minima problems.
2. We propose a formation control law and avoidance strategy for fixed-wing UAVs based on the improved APF method to deal with uncertain and complex environments in a coordinated way. Eventually, under the proposed control law, the formation system can form the desired formation without collisions occurring during UAVs flying process.

The rest of the paper is organized as follows: In section "Modeling," we model the light transmission, APF, and fixed-wing UAV with flight constraints. Section "Avoidance strategy of fixed-wing UAVs" describes the obstacle avoidance strategy of fixed-wing UAVs. In section "Formation obstacle avoidance control law," we design the control law of formation with obstacle avoidance. Simulations are presented in section "Simulations" and followed by concluding remarks in section "Simulations."

Modeling

LTM

In a dense bird flock, each bird feels the least threat of collision when located at the flock border, which is because of the greatest brightness and the strongest light transmission there. On the contrary, the birds in the center feel the most threat of collision. Since the bird moves closer to the boundary of the flock, the brightness that they can feel is gradually strengthened, and the light transmission is proportionately strengthened. Therefore, we can construct the following candidate LTM, which is divided into different cases based on the number of obstacles that the UAVs might encounter.

Assumption 1. To solve the problem of UAV collision avoidance in the obstacle environment, the obstacle in the two-dimensional (2D) space is simplified as a particle, which repulsive action range to UAV is a circle. And the center points of n' obstacles are denoted as $\hat{\boldsymbol{q}}_{\boldsymbol{o}}$ $(o = 1, 2, ..., n')$.

Single obstacle. Consider the 2D obstacle avoidance problem with UAV set $U = \{U_1, U_2, ..., U_N\}$. In Figure 1, we show two possible cases in the process of UAV obstacle avoidance. In Figure 1(a), we assume that at any given time, the ith UAV U_i might fall into the situation where an obstacle blocks the motion of U_i. Therefore, the flyable angle of U_i in the free space is

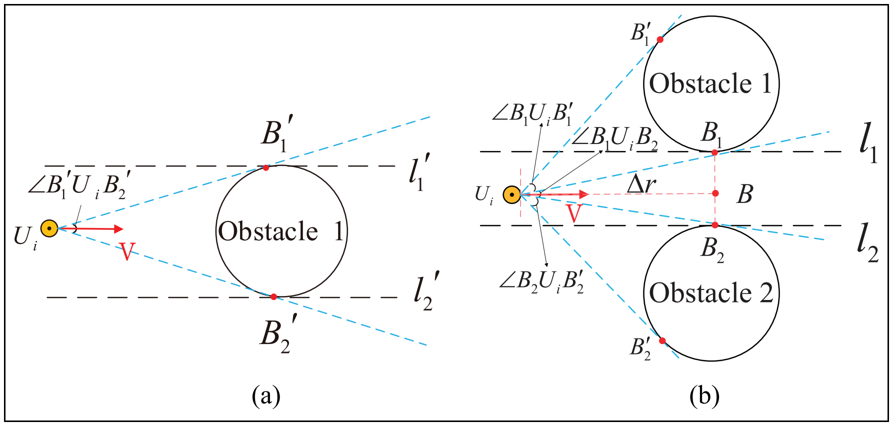

Figure 1. The diagram of UAV collision avoidance: in (a), l_1' and l_2' are the tangent lines of Obstacle 1 along with UAV (U_i), which intersection points with Obstacle 1 are tangent points B_1' and B_2', respectively. In (b), l_1 and l_2 are the tangent lines of Obstacles 1 and 2 along with UAV, respectively, their intersection points are tangent points B_1 and B_2; B_1' is the other tangent point of Obstacle 1 and B_2' is the other tangent point of Obstacle 2. Point B is the intersection of the extension line of UAV speed direction and the connection line of two obstacles; Δr means the length of line segment U_iB.

$$A(U_i) = 2\pi - \angle B_1{}'U_iB_2{}' \tag{1}$$

here, the free space is the flyable space with certain light transmission to the UAV.

Multiple obstacles. In Figure 1(b), assume that there are two obstacles separated with an interval blocking the forward of U_i, and the UAV can fly through their gap to avoid obstacle according to its flight constraints. So, the angle of U_i in the free space in the 2D plane is

$$A(U_i) = \angle B_1U_iB_2 + \pi - \angle B_1U_iB_1' - \angle B_2U_iB_2' \tag{2}$$

According to the light transmission characteristics of birds, the UAV will choose the direction with the strongest light transmission to fly, which range of flight corresponding to this direction is called free motion angle. To cover more possibilities, we can decompose the multi-obstacle environment ($n' > 2$, n' is the number of detectable obstacles for U_i) into cases of choosing the free motion angle of U_i with maximum value, and assigned this value to $A(U_i)$.

The LTM can be considered as the probability $P'(U_i)$ of U_i entering the free space. The event of U_i entering the free space in a 2D plane follows a uniform distribution on $[0, 2\pi]$. Define the candidate LTM as

$$P'(U_i) = \frac{A(U_i)}{2\pi} \tag{3}$$

Considering the LTM defined in equation (3) is only suitable for the situation of partial transmission such as in Figure 1, not for the situation in Figure 2 which will result in U_i to a wrong path called dead-end channel (arrive at point P). Here, partial transmission can be understood as the UAV can detect the feasible routes with certain light transmission, when the obstacles are in front of it. And the flyable space of the UAV decreases as the distance between the UAV and obstacle decreases. When the flyable space of the UAV approaches zero, it can be considered that the UAV has entered the dead-end channel. So, the candidate LTM is needed to be improved by adding a distance factor, which can be defined as

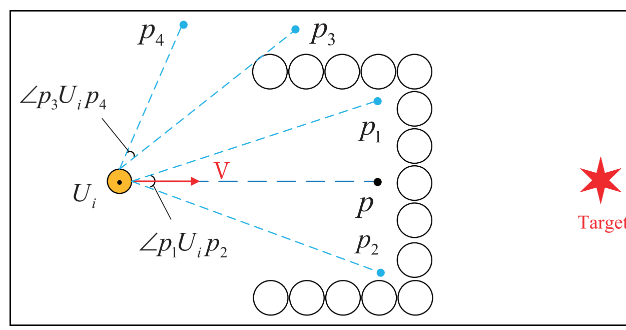

Figure 2. Situation of partial transparent: during the flight, the UAV will not change its course when it detects strong light transmission ahead, that is, the UAV will continue to travel within the range of $\angle p_1U_ip_2$ instead of $\angle p_3U_ip_4$. When the UAV reaches point P, it cannot turn to avoid obstacles because limited by the minimum turning radius and surrounding environment.

$$\xi = e^{\delta \Delta r} \tag{4}$$

where δ is the weight coefficient of distance factor ($\delta > 0$). Obviously, the larger value of δ, the greater influence of the distance factor on the LTM, and vice versa. Δr is the distance from U_i to the detectable obstacle and can be expressed as

$$\Delta r = \begin{cases} \sqrt{(x_{ig} - x_i)^2 + (y_{ig} - y_i)^2}, n' = 1 \\ \sqrt{(x_{ij} - x_i)^2 + (y_{ij} - y_i)^2}, n' \geqslant 2 \end{cases} \tag{5}$$

where (x_i, y_i) is the coordinates of U_i at a certain moment; (x_{ig}, y_{ig}) is the coordinates of the obstacle in only one obstacle case; (x_{ij}, y_{ij}) is the coordinates of the vertical intersection of two adjacent obstacles in more than two obstacles cases, which is like point B in Figure 1(b).

Limited by UAV hardware system, Δr should satisfy the following constraints

$$0 \leqslant \Delta r \leqslant \Delta r_{max} \tag{6}$$

where Δr_{max} means the longest distance U_i of detecting obstacles. Then, combining the candidate LTM in equation (3) with the distance factor in equation (4), we can get the final LTM as

$$P(U_i) = P'(U_i)\xi = \frac{A(U_i)}{2\pi} e^{\delta\Delta r} = \begin{cases} 1 & , n' = 0 \\ \frac{2\pi - \angle B_1{}' U_i B_2{}'}{2\pi} e^{\delta\Delta r} & , n' = 1 \\ \frac{\angle B_1 U_i B_2}{2\pi} e^{\delta\Delta r} & , n' \geqslant 2 \end{cases} \tag{7}$$

where $A(U_i) \in [0, 2\pi]$; $\delta > 0$; $0 \leqslant \Delta r \leqslant \Delta r_{\max}$; $\xi > 1$. In this way, the proposed LTM is associated with the obstacles number, the free space size, and the distance to obstacles.

Avoidance model

To overcome the drawbacks of conventional APF method such as local minima and non-reachable problems, the LTM is introduced to the avoidance model to improve the conventional APF method, which can achieve a better control effect in the formation control.

Obstacle avoidance model.

1. Attractive field function

Define $z_{ij} = ||\boldsymbol{q_i} - \boldsymbol{q_j}||$, and the attractive field function $U_{att}(\boldsymbol{z_{ij}})$ can be expressed as

$$U_{att}(\boldsymbol{z_{ij}}) = \begin{cases} \sum_{j \in \Gamma_i} \frac{k_a}{2} w_1 \cdot \boldsymbol{z_{ij}}^2 & \text{if } \boldsymbol{z_{ij}} \in \tilde{\boldsymbol{D}} \\ 0 & \text{if } \boldsymbol{z_{ij}} \notin \tilde{\boldsymbol{D}} \end{cases} \tag{8}$$

where $w_1 = 1 + k_{p1}P(U_i)$; $\boldsymbol{q_j}$ is the position of the jth UAV; k_a is the attractive factor for changing the intensity of the attractive potential field; $P(U_i)$ is the LTM; k_{p1} is the correlation coefficient of the LTM; when the distance between any two UAVs is within the communication interaction range, we can consider them to be adjacent UAVs, and record this set as Γ_i; and $\tilde{\boldsymbol{D}}$ is the area of flight airspace with a target.

2. Repulsion field function

Define $\tilde{z}_{io} = ||\boldsymbol{q_i} - \boldsymbol{q_o}||$, and the repulsion field function $U_{rep}(\tilde{\boldsymbol{z}}_{io})$ can be expressed as

$$U_{rep}(\tilde{\boldsymbol{z}}_{io}) = \begin{cases} w_2 \frac{b_0}{e^{\frac{\tilde{z}_{io}}{c_0}} - e^{\frac{||q_{io}||_{min}}{c_0}}} & \text{if } \tilde{\boldsymbol{z}}_{io} \in \boldsymbol{D} \\ 0 & \text{if } \tilde{\boldsymbol{z}}_{io} \notin \boldsymbol{D} \end{cases} \tag{9}$$

where $w_2 = 1 + k_{p2}/P(U_i)$; b_0 and c_0 are the constants; k_{p2} is the correlation coefficient of the LTM; $||\boldsymbol{q_{io}}||_{min}$ is the limit safety distance, the UAV will be subjected to repulsive force when the distance between UAV and obstacle is less than this value; D is the airspace, where U_i will be repelled by obstacles; and $\boldsymbol{q_o}$ is the position of oth obstacle.

Collision avoidance model. In UAV formation, leader–following formation is the most common strategy, and the key to this approach is maintaining the relative position and velocity between leader and followers. Using this approach, UAVs can maintain the form in the case of no obstacle; but the formation will be disbanded to avoid obstacles in the case of obstacles, and the previous relative position cannot be maintained.

Therefore, it is necessary to consider the problem of collision avoidance between UAVs formation. To solve this problem, we propose a method that identifies the members of the formation as obstacles with virtual repulsion force, which can prevent UAVs in the formation from colliding with each other or even a chain collision problem in close contact.

Define the repulsion field function between UAVs $U_{rep}(\boldsymbol{z_{ij}})$ expressed as

$$U_{rep}(\boldsymbol{z_{ij}}) = \begin{cases} w_3 \frac{b_1}{e^{\frac{z_{ij}}{c_1}} - e^{\frac{||q_{io}||_{min}}{c_1}}} & \text{if } \boldsymbol{z_{ij}} \in \boldsymbol{D} \\ 0 & \text{if } \boldsymbol{z_{ij}} \notin \boldsymbol{D} \end{cases} \tag{10}$$

where $w_3 = 1 + k_{p3}/P(U_i)$; b_1 and c_1 are the constants; k_{p3} is the correlation coefficient of the LTM.

For convenience, define $\boldsymbol{z_{io}} = ||\boldsymbol{q_i} - \hat{\boldsymbol{q}}_{\boldsymbol{o}}||$, where $\hat{\boldsymbol{q}}_{\boldsymbol{0}}$ is the position of the oth obstacle. Here, the obstacle set consists of real obstacles and its neighbor UAVs assumed as obstacles.

Definition 1. Define $P(U_i) = 0$ when the ith UAV collides with the oth obstacle, which can be expressed as

$$\boldsymbol{q_i}(t) = \hat{\boldsymbol{q}}_{\boldsymbol{o}}(t)$$

where $\boldsymbol{q_i}(t)$ is the position of the ith UAV at time t; $\hat{\boldsymbol{q}}_{\boldsymbol{o}}(t)$ is the position of the oth obstacle at time t ($i = 1, 2, ..., N$; $o = 1, 2, ..., n'$).

Non-reachable and local minima problems. The UAV will fall into the non-reachable point and local minima area when the attractive and repulsive resultant forces are zero. Here, these problems can be solved by changing the weight of the LTM in the repulsive and attractive field functions.

Definition 2. The ith UAV is known as be caught in the non-reachable or local minima when the position $\boldsymbol{q_i}(t-1)$ of the ith UAV at time $t-1$ and the position $\boldsymbol{q_i}(t)$ at time t satisfy

$$||\boldsymbol{q_i}(t) - \boldsymbol{q_i}(t-1)|| < \lambda \tag{11}$$

where λ is the threshold of the distance.

The weight of the LTM in equations (8)–(10) will increase when the ith UAV is caught in non-reachable point or local minima, where $k_{p1} > 1$, $k_{p2} > 1$, and $k_{p3} > 1$ at time t. Here,

Algorithm 1. Step of solving non-reachable or local minima.

Input: $\mathbf{q_i}(t)$, $\mathbf{q_i}(t-1)$, λ
Output: the result of judgment
while Not reaching the target **do**
  if $\|\mathbf{q_i}(t)-\mathbf{q_i}(t-1)\|<\lambda$ **then**
    The *i*th UAV is caught in a local minimum or unreachable point, the force of the *i*th UAV at this time is as follows:[1]
    $f_i = f_{att} + f_{rep} + f_t = 0$
    To solve the above problems, we add the weight of LTM in equations (8)–(10), namely, add the value of $k_{p1}, k_{p2}>1, k_{p3}>1$, and the force of the *i*th UAV after modifying the model is[2]
    $f_i' = f_{att}' + f_{rep}' + f_t'$
    When the LTM weight coefficient in the potential field function is changed, the direction and magnitude of the force on the *i*th UAV will also change, which can help the UAV fly to the direction with the strongest light transmission[3] and escape from the non-reachable point or local minima point.
  else
    UAV normal flight.
  end if
end while

under the APF, the flight direction of the *i*th UAV will be more dependent on LTM. Because the influence of obstacles is considered, it can help the *i*th UAV find feasible free space to escape from the point of non-reachable point or local minima. And the weights will be restored to the original values after the UAV escapes the local minima. The process is shown in Algorithm 1.

UAV model

Suppose that the simplified dynamic model of the *i*th UAV can be expressed as (Wu et al., 2021; Yang et al., 2021)

$$\begin{cases} \dot{x}_i = v_i \cos\psi_i \\ \dot{y}_i = v_i \sin\psi_i \\ \dot{v}_i = n_i^v \\ \dot{\psi}_i = n_i^\psi \end{cases} \tag{12}$$

where (x_i, y_i) is the position of U_i in the inertial coordinate system; ψ_i is the heading angle of U_i; n_i^v and n_i^ψ are the control inputs which represent the overload of the *i*th UAV in inertial coordinate system; v_i is the velocity of U_i.

In order to simplify the *i*th UAV model, we need to linearize equation (12). Define $\boldsymbol{q_i} = [x_i, y_i]^T$, and calculate its first time derivative, we have

$$\boldsymbol{p_i} = \dot{\boldsymbol{q}}_i = \begin{bmatrix} \dot{x}_i \\ \dot{y}_i \end{bmatrix} = \begin{bmatrix} v_i \cos\psi_i \\ v_i \sin\psi_i \end{bmatrix} \tag{13}$$

Furthermore, calculating the first derivative of formula equation (13), we have

$$\begin{aligned} \dot{\boldsymbol{p}}_i = \ddot{\boldsymbol{q}}_i = \begin{bmatrix} \ddot{x}_i \\ \ddot{y}_i \end{bmatrix} \begin{bmatrix} \dot{v}_i \cos\psi_i - v_i\dot{\psi}_i \sin\psi_i \\ \dot{v}_i \sin\psi_i + v_i\dot{\psi}_i \cos\psi_i \end{bmatrix} \\ = \begin{bmatrix} \cos\psi_i & -v_i \sin\psi_i \\ \sin\psi_i & v_i \cos\psi_i \end{bmatrix} \begin{bmatrix} n_i^v \\ n_i^\psi \end{bmatrix} \end{aligned} \tag{14}$$

Then, define

$$\boldsymbol{H_i} = \begin{bmatrix} \cos\psi_i & -v_i \sin\psi_i \\ \sin\psi_i & v_i \cos\psi_i \end{bmatrix} \quad \boldsymbol{n_i} = \begin{bmatrix} n_i^v & n_i^\psi \end{bmatrix}^T$$
$$\boldsymbol{u_i} = \begin{bmatrix} u_i^v & u_i^\psi \end{bmatrix}^T$$

as follows

$$\boldsymbol{u_i} = \boldsymbol{H_i n_i} \tag{15}$$

So, the relationship between the original control input $\boldsymbol{n_i}$ and the new input $\boldsymbol{u_i}$ is as follows

$$\boldsymbol{n_i} = \boldsymbol{H_i}^{-1}\boldsymbol{u_i} \tag{16}$$

Therefore, equations (13) and (14) are transformed into the following second-order integral system

$$\begin{cases} \dot{\boldsymbol{q}}_i = \boldsymbol{p_i} \\ \dot{\boldsymbol{p}}_i = \boldsymbol{u_i} \end{cases} \quad i = 1, 2, \ldots, N \tag{17}$$

where N is the number of UAVs in this formation; and $\boldsymbol{u_i}$ is the control input.

Considering the maneuverability of fixed-wing UAV, the *i*th UAV should satisfy the following group formula of constraint conditions

$$\begin{cases} 0 < v_{min} \leqslant v_i \leqslant v_{max} \\ |w_i| \leqslant w_{max} \\ R_t \geqslant R_{min} \end{cases} \tag{18}$$

where v_{min} and v_{max} represent the minimum and maximum airspeed allowed by all UAVs in fixed altitude flight, respectively; w_i is the heading angular rate of the *i*th UAVs; w_{max} is the maximum allowable heading angular rate of all UAVs; R_t is the turning radius of all UAVs; and n_{max} is the maximum overload of all UAVs, then the minimum turning radius can be expressed as

$$R_{min} = \frac{v_i^2}{n_{max}} \tag{19}$$

Avoidance strategy of fixed-wing UAVs

According to the flight characteristics of the fixed-wing UAV in equation (18), the speed direction of the UAV will be restricted by the following three situations when it flies toward the obstacle area. Correspondingly, avoidance strategies are proposed for these situations.

Situation 1

In Figure 3(a), there are two obstacles with an interval in the front of the *i*th UAV. For this case, the *i*th UAV can always go through the interval with arbitrary incident direction, when $2R_{\min} < d'$ (d' is the interval length between two obstacles) is satisfied.

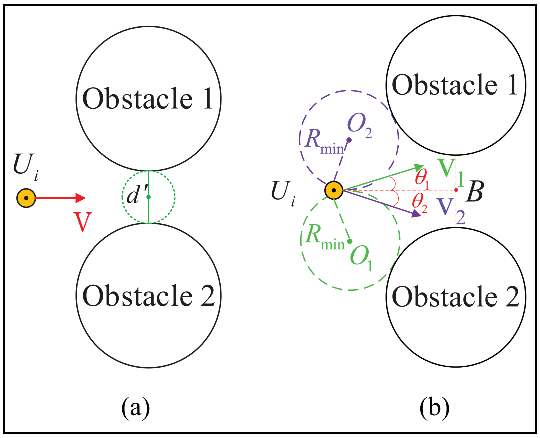

Figure 3. Speed constraint diagram of situation: in (a), the turning radius of the UAV is smaller than the distance between two obstacles. In (b), point B is the intersection of the extension line of horizontal speed direction and the connection line of two obstacles; θ_1 and θ_2 are the angles between the speed direction of the UAV and the line segment U_iB, when O_1 is tangent with the Obstacle 1 and O_2 is tangent with the Obstacle 2, respectively.

Situation 2

Similar to the situation in Figure 3(a), there are also two obstacles with an interval in Figure 3(b). But this time, the interval length between two obstacles is less than twice R_{min}, which means the ith UAV can only go through the interval under a certain incident direction. In Figure 3(b), set a line segment perpendicular to the velocity direction so that its length is $R_{\min}$ and its endpoint is O_1. Then, draw a circle with $R_{\min}$ as the radius and O_1 as the center. In order to prevent the ith UAV from colliding with Obstacle 1, the following conditions should satisfy:

1. If O_1 does not intersect the Obstacle 1, the ith UAV can go through the interval safely.
2. If O_1 and the Obstacle 1 are tangent, the direction of the limit incident angle (θ_1) can be obtained. That is, the incident direction (θ) must satisfy $\theta \leqslant \theta_1$ to avoid the collision.
3. If O_1 intersects the Obstacle 1, the ith UAV will collide with the obstacles.

With the same method, we can get the conditions that prevent the ith UAV from colliding with Obstacle 2. So, the incident direction (θ) should be satisfied $\theta \in [\theta_2, \theta_1]$, where θ_2 is the direction of ultimate incident to avoid Obstacle 2.

Situation 3

Figure 4 shows when the ith UAV is situated in an environment with multiple obstacles, it will decide an appropriate choice of going through one of the intervals between obstacles. Finally, the ith UAV will fly toward the interval with maximum length after comparing. However, there also exists a special case to decide when the transmission probabilities of two feasible choices are equal. In the light of this problem, we make tangent line of adjacent obstacles along the drone position, then $\angle T_1U_iT_2 = \angle T_3U_iT_4$. The angles between along the line of speed direction and the Obstacle's tangent are θ_3 and θ_4. The side with the smaller angle will be chosen by the ith UAV, where considered the principle of the minimum cost of the flight path that the UAV does not change the flight direction as much as possible, or completes obstacle avoidance with the smallest changes to reduce fuel consumption. The process of constraint judgment is given in Algorithm 2.

In brief, the application scenario of the LTM can be obtained based on the above-mentioned conditions, which

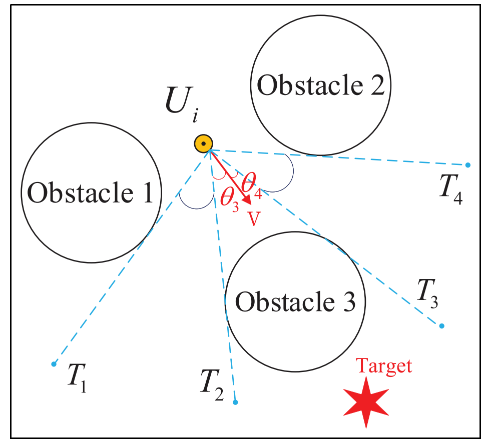

Figure 4. Speed constraint diagram of situation: line U_iT_2 and U_iT_3 are the tangent lines between the UAV and the Obstacle 3; θ_3 and θ_4 are the included angles between the UAV speed direction and line U_iT_2 and U_iT_3, respectively.

Algorithm 2. The step of constraint judgment.

```
Input: v_i
  Output: the result of judgment
    if Only have one feasible path then
      if 2R_min < d' then
        UAV normal flight
      else
        Make ⊙ O_1 and ⊙O_2 to determine θ_1 and θ_2
        if θ ∈ [θ_1, θ_2] then
          UAV normal flight
        else
          Might unable to turn safely (Collision)
        end if
      end if
    else
      if Have equal transmission probabilities then
        if θ_3 > θ_4 then
          Flying towards θ_4
        else
          Flying towards θ_3
        end if
      else
        UAV normal flight
      end if
    end if
```

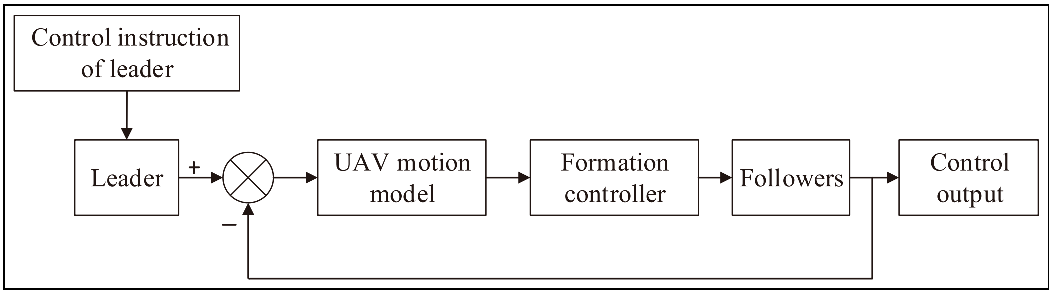

Figure 5. The structure diagram of the formation control system: during the control process, the ground station sends control information (including formation speed, formation shape, navigation target, etc.) to the leader in the formation, and the formation receives the control information and makes corresponding flight actions. As the leader state changes, the followers make corresponding changes under the action of the formation controller to maintain the formation, which can ensure the consistency of the formation. Finally, the state information of the UAVs is used as the control outputs, and also as negative feedback to the formation controller to complete the closed-loop control of formation flight.

can provide an effective strategy for UAV formation to avoid obstacles.

Formation obstacle avoidance control law

Formation control law

In this section, a formation control law is designed as equation (20) to ensure the obstacle avoidance and of UAVs

$$\boldsymbol{u}_i = \boldsymbol{u}_i^{\alpha} + \boldsymbol{u}_i^{\beta} + \boldsymbol{u}_i^{\gamma} \tag{20}$$

where

$$\begin{cases} \boldsymbol{u}_i^{\alpha} = -c_1^{\alpha} \sum\limits_{j\epsilon\Gamma_i} \nabla U_{att}\left(\boldsymbol{z_{ij}}\right) + c_2^{\alpha} \sum\limits_{j\epsilon\Gamma_i} a_{ij}(t)\left(\boldsymbol{p_j} - \boldsymbol{p_i}\right) \\ \boldsymbol{u}_i^{\beta} = -c_1^{\beta} \sum\limits_{o\epsilon\Gamma_o} \nabla U_{rep}(\boldsymbol{z_{io}}) + c_2^{\beta} \sum\limits_{o\epsilon\Gamma_o} (\boldsymbol{\hat{p}_o} - \boldsymbol{p_i}) \\ \boldsymbol{u}_i^{\gamma} = -c_1^{\gamma}\left(\boldsymbol{q}_i - \boldsymbol{q}_{\gamma}\right) - c_2^{\gamma}(\boldsymbol{p}_i - \boldsymbol{p}\gamma) \end{cases}$$

where $c_n^m(n = 1, 2, m = \alpha, \beta, \gamma)$ are the control parameters; $\boldsymbol{p}_i$, $\boldsymbol{p}_j$, and $\boldsymbol{\hat{p}_o}$ represent the speed of the ith UAV, the jth UAV, and the oth obstacle, respectively; $\boldsymbol{q}_{\gamma}$ and $\boldsymbol{p}_{\gamma}$ are the position and the speed of the navigation item; Γ_o is the set of obstacles and the neighbors of the ith UAV considered as obstacles; and a_{ij} is the (i,j) term of the adjacency matrix A.

$\boldsymbol{u}_i^{\alpha}$ is the item for driving the ith UAV to gather with other UAVs, which consists of two parts. One is to maintain the cooperative UAVs with the desired distance, and another is to make the consistent speed of the ith UAV with its neighbors; $\boldsymbol{u}_i^{\beta}$ is used for the ith UAV obstacle avoidance control and $\boldsymbol{u}_i^{\gamma}$ is the navigation item for ith UAV to reach the target position. And the structure diagram of the formation control system is shown in Figure 5.

Analysis of the control law

For a better description of control issues in the UAVs formation, we introduce the following definition at first.

Definition 3. The control goal on formation obstacle avoidance and collision avoidance is that for any time t, the position of the ith UAV and the jth UAV satisfies

$$\| \boldsymbol{q_i}(t) - \boldsymbol{q_j}(t) \| 0 = \nrightarrow 0 \ (i \neq j; i, j = 1, 2, ..., N) \tag{21}$$

and the position of the ith UAV and the oth obstacle satisfies

$$\| \boldsymbol{q_i}(t) - \boldsymbol{\hat{q}_o}(t) \| 0 = \nrightarrow 0 \ (i = 1, 2, ..., N; o = 1, 2, ..., n') \tag{22}$$

Definition 4. If the position of the ith UAV and the jth UAV satisfies

$$\begin{aligned} &\| \boldsymbol{q_i}(\mathbf{t}) - \boldsymbol{q_l}(\mathbf{t}) - \boldsymbol{\varepsilon}_{\mathbf{i}} \| = \| \boldsymbol{q_j}(\mathbf{t}) - \boldsymbol{q_l}(\mathbf{t}) - \boldsymbol{\varepsilon_j} \| \\ &(t > t_k, i \neq j; i, j = 1, 2, ..., N) \end{aligned} \tag{23}$$

where t_k is some time instant; $\boldsymbol{q_l}$ is the position of the leader UAV in formation; $\boldsymbol{\varepsilon}_{\mathbf{i}}$ is the relative position between the ith UAV and the leader UAV; $\boldsymbol{\varepsilon_j}$ is the relative position between the jth UAV and the leader UAV correspondingly. Then, we can consider that the system realizes the desired formation.

Before analyzing whether the formation system can realize the desire formation and avoid the obstacles, we make the following assumptions on the communication condition and system energy of UAV formation.

Assumption 2. The communication radius of the ith UAV is larger than the size of obstacles, which means we do not take into account the impact of obstacles on the communication quality between UAVs. In other words, the communication digraph $G(A)$ of the formation system is connected during the whole process.

Assumption 3. For the formation system composed of N UAVs, the total energy of this system is a value finite at any time t, that is

$$W(t) \leqslant W_0$$

where $W(t)$ is the value of system energy at time t, and W_0 is a given value.

Before giving the main result, we next introduce a well-known lemma on system stability.

Lemma 1. Let V: $\mathbb{R}^n \rightarrow \mathbb{R}$ be a locally positive definite function such that on the compact set $\Omega_c = x \in \mathbb{R}^n : V(x) \leqslant C$ (C is a constant greater than zero), we have $\dot{V}(x) \leqslant 0$ (Shevitz and Paden (1994) (LaSalle's principle)). Define

$$S = x \in \Omega_c : \dot{V}(x) = 0 \tag{24}$$

As $t \rightarrow \infty$, the trajectory tends to the largest invariant set inside S. In particular, if S contains no invariant sets other than $x = 0$, then 0 is an only equilibrium point.

Based on the above preparation, we are ready to analyze the stability of the formation system.

Theorem 1. Consider a formation system composed of N UAVs with the characteristics of equation (17). If Assumptions 2 and 3 hold, under the control law of equation (20), the formation system will form the desired formation eventually, while ensuring that no collisions occur for the ith UAV and other UAVs during their flying process.

Proof. Define the system energy function as

$$W = \frac{1}{2}\sum_{i=1}^{N}\left[F_i + \left(\boldsymbol{p}_i - \boldsymbol{p}_\gamma\right)^T\left(\boldsymbol{p}_i - \boldsymbol{p}_\gamma\right)\right] \tag{25}$$

where

$$F_i = \left(c_1^\alpha V_i^\alpha + c_1^\beta V_i^\beta\right) + 2c_1^\gamma\left(\boldsymbol{q_i} - \boldsymbol{q}_\gamma\right)^T\left(\boldsymbol{q_i} - \boldsymbol{q}_\gamma\right) \tag{26}$$

$$V_i^\alpha = \sum_{i \epsilon \Gamma_i} U_{att}\left(\boldsymbol{z_{ij}}\right) \tag{27}$$

$$V_i^\beta = \sum_{o \epsilon \Gamma_o} U_{rep}\left(\boldsymbol{z_{io}}\right) \tag{28}$$

Denote $\tilde{\boldsymbol{q}}_i = \boldsymbol{q}_i - \boldsymbol{q}_\gamma$, so we have $\|\boldsymbol{q_i} - \boldsymbol{q_j}\| = \|\tilde{\boldsymbol{q}}_i - \tilde{\boldsymbol{q}}_j\|$ and $\|\boldsymbol{q_i} - \hat{\boldsymbol{q}}_o\| = \|\tilde{\boldsymbol{q}}_i - \tilde{\hat{\boldsymbol{q}}}_o\|$. Then, F_i in equation (26) can be rewritten as

$$F_i = \left(c_1^\alpha V_i^\alpha + c_1^\beta V_i^\beta\right) + 2c_1^\gamma\left(\tilde{\boldsymbol{q}}_i^T\tilde{\boldsymbol{q}}_i\right) \tag{29}$$

Differentiate two sides of equation (29) with respect to time t, we have

$$\begin{aligned}\sum_{i=1}^{N}\dot{F}_i &= c_1^\alpha\Big[\dot{\tilde{\boldsymbol{q}}}_i^T\nabla U_{att}\left(\|\tilde{\boldsymbol{q}}_i - \tilde{\boldsymbol{q}}_j\|\right) \\ &\quad + \dot{\tilde{\boldsymbol{q}}}_j^T\nabla U_{att}\left(\|\tilde{\boldsymbol{q}}_i - \tilde{\boldsymbol{q}}_j\|\right)\Big] \\ &\quad + 2c_1^\gamma\sum_{i=1}^{n}\dot{\tilde{\boldsymbol{q}}}_i^T\tilde{\boldsymbol{q}}_i \\ &\quad + c_1^\beta\Big[\dot{\tilde{\boldsymbol{q}}}_i^T\nabla U_{rep}\left(\|\tilde{\boldsymbol{q}}_i - \tilde{\hat{\boldsymbol{q}}}_o\|\right) \\ &\quad + \dot{\tilde{\hat{\boldsymbol{q}}}}_o^T\nabla U_{rep}\left(\|\tilde{\boldsymbol{q}}_i - \tilde{\hat{\boldsymbol{q}}}_o\|\right)\Big] \\ &= 2c_1^\alpha\sum_{i=1}^{N}\dot{\tilde{\boldsymbol{q}}}_i^T\nabla V_i^\alpha + 2c_1^\beta\sum_{i=1}^{N}\dot{\tilde{\boldsymbol{q}}}_i^T\nabla V_i^\beta \\ &\quad + 2c_1^\gamma\sum_{i=1}^{n}\dot{\tilde{\boldsymbol{q}}}_i^T\tilde{\boldsymbol{q}}_i\end{aligned} \tag{30}$$

Because $\boldsymbol{p}_\gamma$ is assumed to be a constant, we have $\dot{\tilde{\boldsymbol{p}}}_i = \dot{\boldsymbol{p}}_i - \dot{\boldsymbol{p}}_\gamma = \dot{\boldsymbol{p}}_i = \boldsymbol{u}_i$, and $\dot{\tilde{\boldsymbol{q}}}_i = \tilde{\boldsymbol{p}}_i = \boldsymbol{p}_i - \boldsymbol{p}_\gamma$. And substitute the expressions of $\dot{\tilde{\boldsymbol{p}}}_i$ and $\dot{\tilde{\boldsymbol{q}}}_i$ into equation (30), the time derivative of energy function is given as follows

$$\begin{aligned}\dot{W} &= \frac{1}{2}\sum_{i=1}^{N}\dot{F}_i + \frac{1}{2}\sum_{i=1}^{N}\left(\tilde{\boldsymbol{p}}_i^T\dot{\tilde{\boldsymbol{p}}}_i + \dot{\tilde{\boldsymbol{p}}}_i^T\tilde{\boldsymbol{p}}_i\right) \\ &= \frac{1}{2}\sum_{i=1}^{N}\dot{F}_i + \sum_{i=1}^{N}\tilde{\boldsymbol{p}}_i^T\boldsymbol{u}_i \\ &= \sum_{i=1}^{N}\tilde{\boldsymbol{p}}_i^T\left[c_1^\alpha\nabla V_i^\alpha + c_1^\beta\nabla V_i^\beta + c_1^\gamma\tilde{\boldsymbol{q}}_i + \boldsymbol{u}_i\right] \\ &= \sum_{i=1}^{N}\tilde{\boldsymbol{p}}_i^T\Big[c_1^\alpha\nabla V_i^\alpha + c_1^\beta\nabla V_i^\beta + c_1^\gamma\tilde{\boldsymbol{q}}_i \\ &\quad - c_1^\alpha\nabla V_i^\alpha + c_2^\alpha\sum_{j\in\Gamma_i}a_{ij}(t)\left(\tilde{\boldsymbol{p}}_j - \tilde{\boldsymbol{p}}_i\right) \\ &\quad - c_1^\beta\nabla V_i^\beta + c_2^\beta\sum_{o\in\Gamma_o}\left(\tilde{\hat{\boldsymbol{p}}}_o - \tilde{\boldsymbol{p}}_i\right) - c_1^\gamma\tilde{\boldsymbol{q}}_i - c_2^\gamma\tilde{\boldsymbol{p}}_i\Big] \\ &= \sum_{i=1}^{N}\tilde{\boldsymbol{p}}_i^T\Big[c_2^\alpha\sum_{j\in\Gamma_i}a_{ij}(t)\left(\tilde{\boldsymbol{p}}_j - \tilde{\boldsymbol{p}}_i\right) \\ &\quad + c_2^\beta\sum_{o\in\Gamma_o}\left(\tilde{\hat{\boldsymbol{p}}}_o - \tilde{\boldsymbol{p}}_i\right) - c_2^\gamma\tilde{\boldsymbol{p}}_i\Big] \\ &= \underbrace{\sum_{i=1}^{N}\tilde{\boldsymbol{p}}_i^Tc_2^\alpha\sum_{j\in\Gamma_i}a_{ij}(t)\left(\tilde{\boldsymbol{p}}_j - \tilde{\boldsymbol{p}}_i\right)}_{term1} \\ &\quad + \underbrace{\sum_{i=1}^{N}\tilde{\boldsymbol{p}}_i^Tc_2^\beta\sum_{o\in\Gamma_o}\left(\tilde{\hat{\boldsymbol{p}}}_o - \tilde{\boldsymbol{p}}_i\right)}_{term2} - \sum_{i=1}^{N}\tilde{\boldsymbol{p}}_i^Tc_2^\gamma\tilde{\boldsymbol{p}}_i\end{aligned} \tag{31}$$

Under the action of the new force generated by the repulsion field, the ith UAV approaching the oth obstacle will generate a new speed component, which can be defined as

$$\hat{\boldsymbol{p}}_o = \boldsymbol{p}_i - \Lambda_j\Lambda_j^T\boldsymbol{p}_i + \Lambda_j\Lambda_j^T\boldsymbol{p}_\gamma \tag{32}$$

where

$$\Lambda_j = \begin{cases}\dfrac{\boldsymbol{q_i} - \hat{\boldsymbol{q}}_o}{\|\boldsymbol{q_i} - \hat{\boldsymbol{q}}_o\|} & , \|\boldsymbol{q_i} - \hat{\boldsymbol{q}}_o\| \neq 0 \\ 0 & , otherwise\end{cases} \tag{33}$$

So, we have

$$\tilde{\hat{\boldsymbol{p}}}_o = \hat{\boldsymbol{p}}_o - \boldsymbol{p}_\gamma = \tilde{\boldsymbol{p}}_i - \Lambda_j\Lambda_j^T\tilde{\boldsymbol{p}}_i \tag{34}$$

Follows from equation (34), term 2 in equation (31) can be rewritten as

$$\sum_{i=1}^{N}\tilde{\boldsymbol{p}}_i^T\left[c_2^\beta\sum_{j\in\Gamma_o}\left(\tilde{\hat{\boldsymbol{p}}}_o - \tilde{\boldsymbol{p}}_i\right)\right] = -c_2^\beta\sum_{j\in\Gamma o}\left(\Lambda_j^T\tilde{p}_i\right)^2 \leqslant 0 \tag{35}$$

Similar to equation (32), we have

$$\boldsymbol{p}_j = \boldsymbol{p}_i - \tilde{\Lambda}_j \tilde{\Lambda}_j^T \boldsymbol{p}_i + \tilde{\Lambda}_j \tilde{\Lambda}_j^T \boldsymbol{p}_\gamma \tag{36}$$

where having

$$\tilde{\Lambda}_j = \begin{cases} \frac{\boldsymbol{q}_i - \boldsymbol{q}_j}{\|\boldsymbol{q}_i - \boldsymbol{q}_j\|} & , \|\boldsymbol{q}_i - \boldsymbol{q}_j\| \neq 0 \\ 0 & , otherwise \end{cases} \tag{37}$$

So, we have

$$\tilde{\boldsymbol{p}}_j = \boldsymbol{p}_j - \boldsymbol{p}_\gamma = \tilde{\boldsymbol{p}}_i - \tilde{\Lambda}_j \tilde{\Lambda}_j^T \tilde{\boldsymbol{p}}_i \tag{38}$$

Follows from equation (38), term 1 in equation (31) can be rewritten as

$$\begin{aligned} &\sum_{i=1}^{N} \tilde{\boldsymbol{p}}_i^T \left[c_2^\alpha \sum_{j \in \Gamma_i} a_{ij}(t) \left(\tilde{\boldsymbol{p}}_j - \tilde{\boldsymbol{p}}_i \right) \right] \\ &= -c_2^\alpha \sum_{j \in \Gamma_i} a_{ij}(t) \left(\tilde{\Lambda}_j^T \tilde{\boldsymbol{p}}_i \right)^2 \leqslant 0 \end{aligned} \tag{39}$$

Considering that $c_2^\alpha, c_2^\beta, c_2^\gamma$, and a_{ij} are all greater than 0, combining equations (31), (35) and (39), we can get

$$\dot{W} \leqslant 0 \tag{40}$$

From equation (40), we know that W is a non-increasing function. According to Assumption 3, for any time t, we have

$$W(t) \leqslant W_0 \tag{41}$$

then, according to Assumption 2, if graph G is connected, there must be a connected path between node i and node j in graph G. In this way, it can be known that the distance between the ith UAV and the jth UAV is bounded, that is, $\boldsymbol{z_{ij}}$ is a bounded vector. So, we can get the set $\Omega = \boldsymbol{z_{ij}} | W(t) \leqslant W_0, t > 0$ is a positively invariant compact set. According to Lemma 1, every solution in Ω tends to the largest invariant set, such that

$$E = \boldsymbol{z_{ij}} \in \Omega | \dot{W}(t) = 0 \tag{42}$$

In equation (42), $\dot{W}(t) = 0$ means that the energy of the system does not change with time, that is, the formation system goes into an equilibrium. For system equation (17), all the UAVs will enter the corresponding position of the formation eventually. And the position relationship between the UAVs satisfies equation (23).

Therefore, we know the formation system will finally form the desired formation under the action of the control law of equation (20).

Next, proof by contradiction is used to prove that the UAVs in the formation system will not collide with obstacle at any time. Suppose that there is at least one UAV U_r colliding with the oth obstacle at time t_1 ($t_1 > 0$) in the formation system, where the positions of the rth UAV and the oth obstacle at time t_1 satisfy

$$\boldsymbol{q_r}(t_1) = \hat{\boldsymbol{q}}_{\boldsymbol{o}}(t_1) \tag{43}$$

Combining the definition of repulsion field function in equation (9) and Definition 1, we can obtain the value of repulsion field for U_r, which tends to the infinite, namely

$$V_r^\beta \to \infty \tag{44}$$

Substituting equation (44) to equation (25), we obtain

$$\frac{1}{2} \sum_{i=1}^{N} F_i \to \infty \tag{45}$$

However, combining equation (25) with Assumption 3, we have

$$\begin{aligned} \frac{1}{2} \sum_{i=1}^{N} F_i &= W - \frac{1}{2} \sum_{i=1}^{N} \left[\left(\boldsymbol{p}_i - \boldsymbol{p}_\gamma \right)^T \left(\boldsymbol{p}_i - \boldsymbol{p}_\gamma \right) \right] \\ &\leqslant W \leqslant W_0 \end{aligned} \tag{46}$$

which leads to a contradiction with equations (43)–(45).

So, the above suppose does not hold, which implies that there exists no collision for the ith UAV with the oth obstacles during the flying process. In this way, the position relationship in equation (22) is satisfied. As before, we identify the other UAVs as obstacles. So, the proof of the position relationship in equation (21) is similar to the proof of equation (22), which is omitted.

Finally, we obtain that under the control law in equation (20), the formation system can achieve obstacle avoidance and collision avoidance control.

Simulations

In this part, we conducted simulations to illustrate the effectiveness of the proposed obstacle avoidance control law, where also compared it with the conventional APF method correspondingly to show the superiority of the proposed method. The formation is made up of five UAV members, including one leader and four followers. Assume that the communication graph of UAVs is shown in Figure 6, which is leader–following formation.

Define the communication graph is $G = (V, E, A)$, where V is a non-empty set called the vertex set of G; E is the edge set

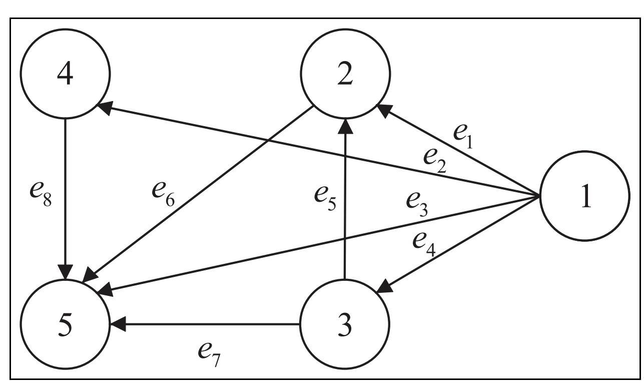

Figure 6. The communication graph and desired formation of UAVs.

of G whose elements are edges; A is the adjacency matrix and L is the Laplacian matrix

$$A = \begin{bmatrix} 0 & 1 & 1 & 1 & 1 \\ 0 & 0 & 0 & 0 & 1 \\ 0 & 1 & 0 & 0 & 1 \\ 0 & 0 & 0 & 0 & 1 \\ 0 & 0 & 0 & 0 & 0 \end{bmatrix}, \quad L = \begin{bmatrix} 0 & -1 & -1 & -1 & -1 \\ 0 & 2 & 0 & 0 & -1 \\ 0 & -1 & 1 & 0 & -1 \\ 0 & 0 & 0 & 1 & -1 \\ 0 & 0 & 0 & 0 & 4 \end{bmatrix}$$

Formation control without obstacles

In this simulation, the proposed formation control algorithm based on improved APF method is verified.

Here, assume there exists no obstacle in airspace. The target point is set in (15,15) and the UAVs have different initial positions. Set the desired interval between UAV followers and leader is $\boldsymbol{\varepsilon_1} = [-1.5\ 1.5]^T$, $\boldsymbol{\varepsilon_2} = [-1.5\ -1.5]^T$, $\boldsymbol{\varepsilon_3} = [-3\ 1.5]^T$, and $\boldsymbol{\varepsilon_4} = [-3\ -1.5]^T$, respectively. When the simulation begins, the UAVs will form the desired formation and move coordinately. And the key simulation parameters in this system are as follows: the distance factor $\delta = 0.45$; the minimum turning radius $R_{min} = 0.5\,\text{m}$; the maximum overload $n_{max} = 10\,\text{G}$; the LTM coefficient $k_{p1} = 0.3$, $k_{p2} = 0.5$, and $k_{p3} = 0.1$, respectively. Here, there is no obstacle in the airspace and the LTM coefficients k_{p1}, k_{p2} can be understood as artificial initial setting parameters, which will remain unchanged during the whole process and will not affect the flight of the UAV.

It is worth noting that the key simulation parameters are comprehensively determined based on the flight path distance, the size and number of obstacles, the preset simulation performance of the UAV (speed, minimum turning radius, overload, communication distance, etc.), formation shape, and so on, which need to make the parameters conform to the physical logic and has the value of simulation research. Specifically, some of the following rules can be followed:

1. Within a certain range, the light transmission of the UVA can be enhanced via adding the weight of the distance factor in the LTM.
2. In order to ensure the shape of the formation, the LTM coefficient k_{p3} should be decreased with the density of formation increasing.
3. The larger the values of the LTM coefficient k_{p1} and k_{p2} are, the greater the influence of the LTM on the UAV in the potential field function is.
4. The smaller the turning radius of the UAV is, the easier the UAV avoids obstacles in a short time.

In addition, according to different experimental environments, the trial-and-error method is occasionally adopted to determine the simulation parameters of the optimal effect.

The computer used in the simulation in this paper is equipped with Intel Core i5-9300H-class CPU, 16 GB memory, and 512 GB solid-state hard disk. And the average running speed of the experiment is 0.35 seconds, and the average CPU utilization rate is 8%.

The simulation results in Figure 7 show that the designed communication structure and control law have good consistency in UAV formation flight. The position intervals between the leader and followers tend to desired distances, and the position tracking error of each UAV tends to 0 gradually.

Formation control on obstacle avoidance

In this simulation, the proposed formation control with collision avoidance based on improved APF method is verified, which can be expressed as a process including UAVs forming aggregation, avoiding obstacles in an unknown environment, and reaching the target area. And several obstacles are set on UAV's way to the target. Here, the smoothing constraints are added in the experiments, which fully consider the dynamic model of the fixed-wing UAV (including the constraints of the minimum turning radius). Figure 8 shows the UAVs can

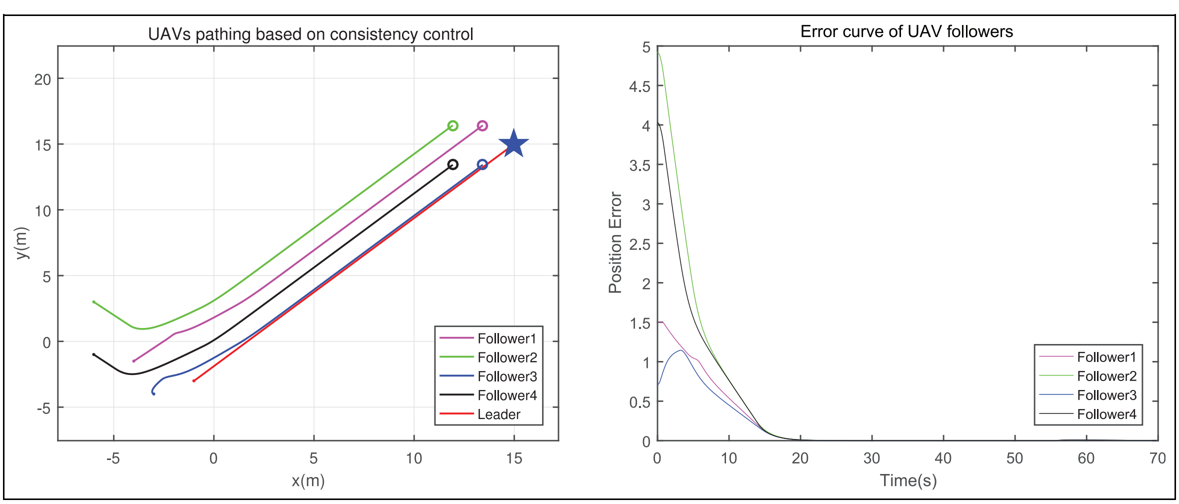

Figure 7. Result of formation consistency control.

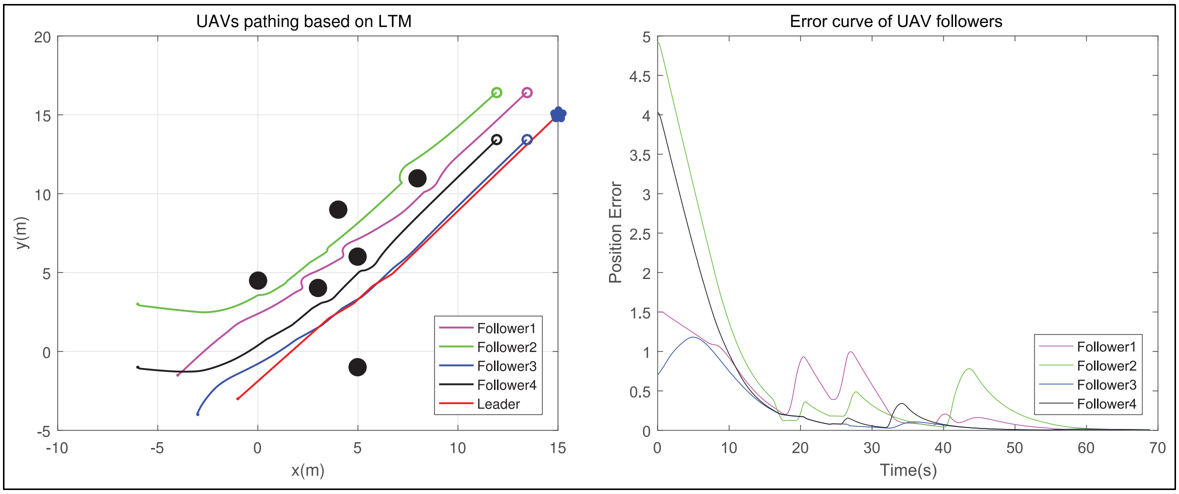

Figure 8. Obstacles avoidance result of improved APF approach.

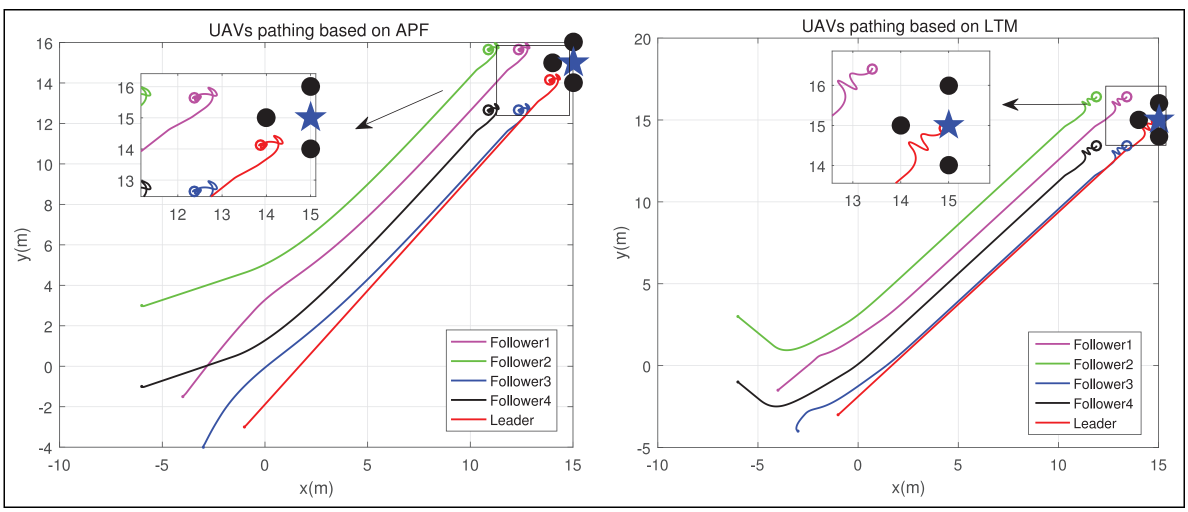

Figure 9. Result of solving non-reachable problem.

avoid obstacles and build up to the full formation. Furthermore, the proposed method is suitable not only for the common problems in Figure 8 but also for some special problems listed from Figures 9–13, which cannot be solved by APF. Here, the simulation parameters are the same as above.

The results in Figures 9 and 10 show that the UAVs can break away from the local minimum and non-reachable point successfully when adopting the LTM to improve the APF method. Figures 11–13 demonstrate the proposed method performs better than the original APF method in some special cases of obstacle avoidance, especially in the multi-obstacle environment. The above numerical results have shown that the proposed method is effective and feasible.

Conclusion

In this paper, a UAV formation obstacle avoidance control method based on LTM and improved APF is proposed. First, the LTM is proposed which is used to combine with the conventional APF function to form an improved APF method. Then, the collision avoidance and obstacle avoidance models of UAVs are introduced. Besides, the corresponding obstacle avoidance strategies of an improved APF method are given in the meantime. Furthermore, the UAV formation obstacle avoidance control law under the leader–following formation is designed. Finally, the simulation results show that the proposed methods have strong reliability and validity which is superior to the existing methods.

Compared with the conventional APF method, the improved APF control method based on the LTM can ensure better the UAV formation to find the maneuvering flight route, and not to collide during the flight process, which can also effectively reduce the limitations of the potential field method. The control method proposed in this paper provides a reliably theoretical support for the actual formation flight, which has a high application prospect. However, this paper

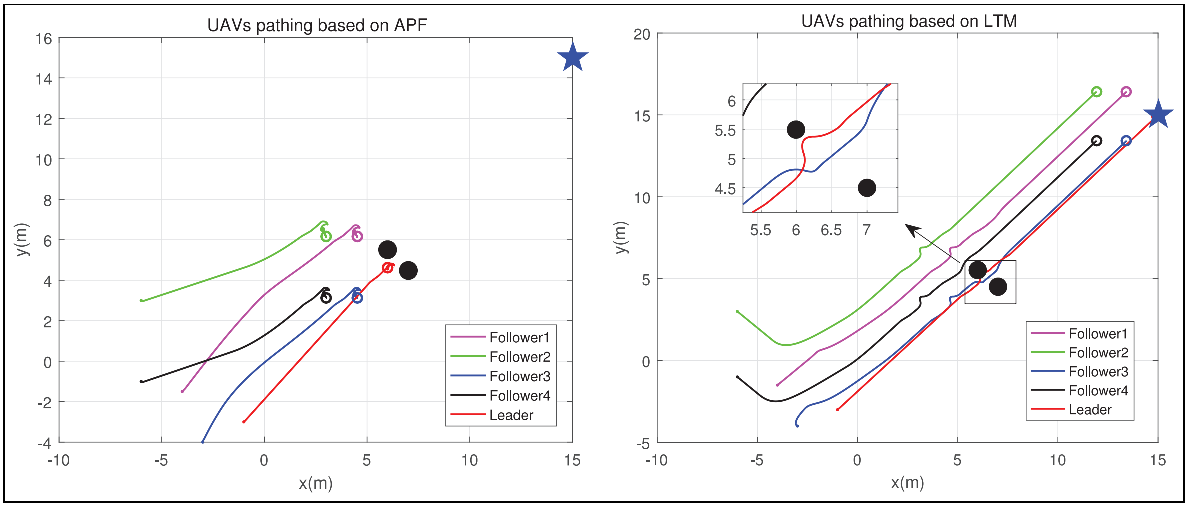

Figure 10. Result of solving local minima problem.

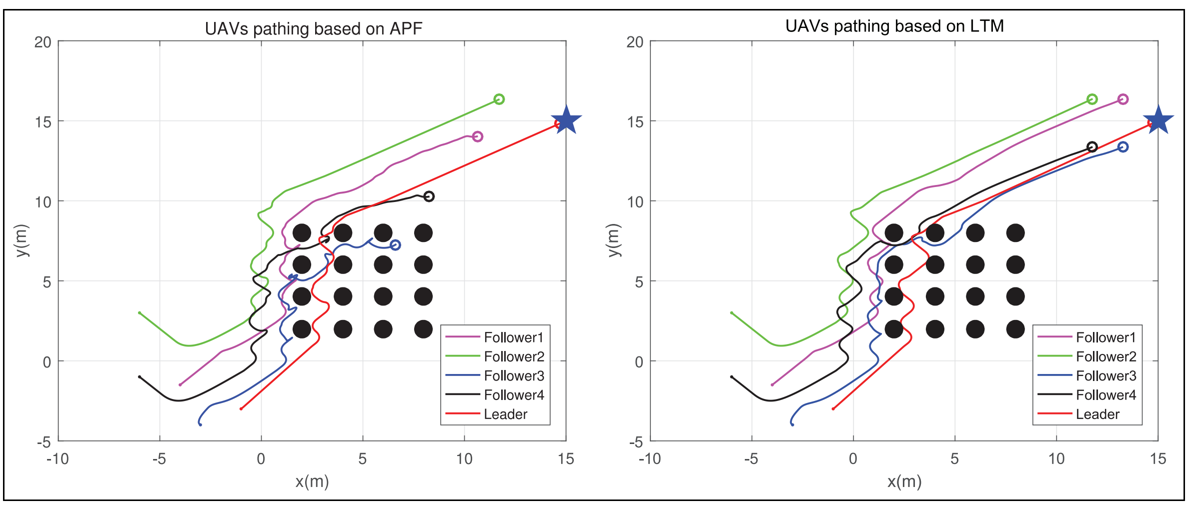

Figure 11. Result of collision avoidance.

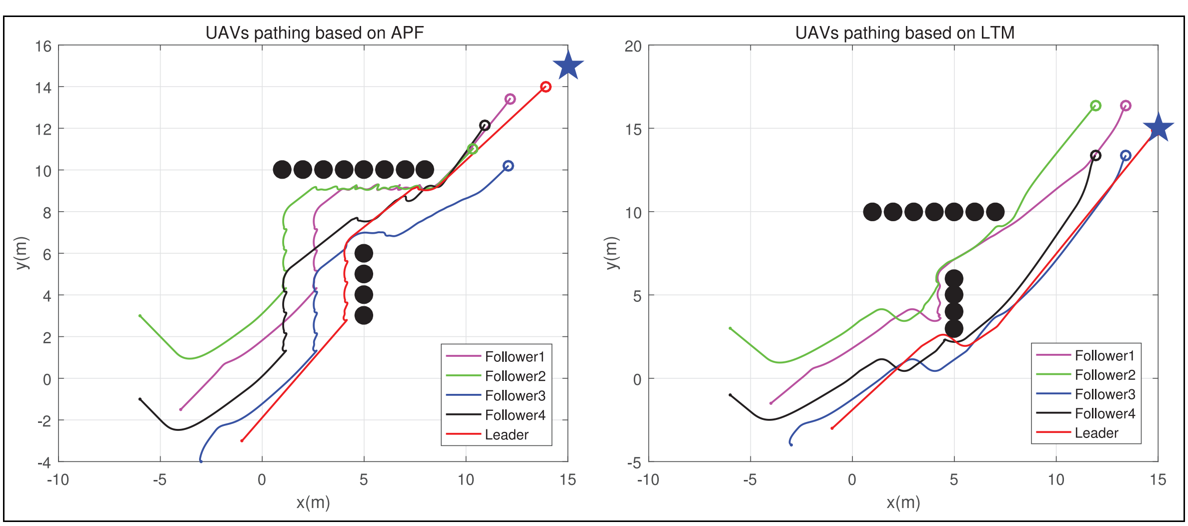

Figure 12. Result of collision avoidance.

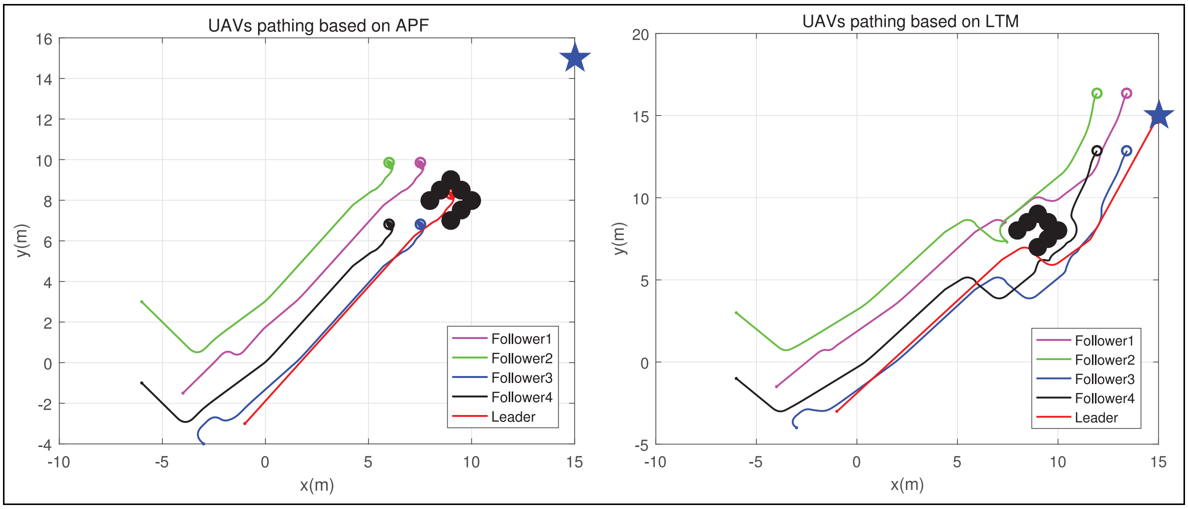

Figure 13. Result of collision avoidance.

only studies a small number of UAVs flying in formation, and in the future research, we will expand the number of UAVs and study the obstacle avoidance control of UAV swarms based on the improved APF method in this paper.

Declaration of conflicting interests

The author(s) declared no potential conflicts of interest with respect to the research, authorship, and/or publication of this article.

Funding

The author(s) disclosed receipt of the following financial support for the research, authorship, and/or publication of this article: This work was supported by the National Natural Science Foundation of China (61973253).

ORCID iD

Jiacheng Li https://orcid.org/0000-0001-8762-0955

Notes

1. f_i is the resultant force on the ith UAV; f_{att} is the attractive force on the ith UAV ($f_{att} = -\nabla U_{att}$); f_{rep} is the repulsive force on the ith UAV ($f_{rep} = -\nabla U_{rep}$); f_t is the force of the navigation item on the ith UAV.
2. $f_i{}', f_{att}{}', f_{rep}{}', f_t{}'$ are the forces after changing the weight of the LTM model.
3. The direction with the strongest light transmission can be selected via the strategy in section "Avoidance strategy of fixed-wing UAVs"; in the direction, the sizes of the light transmission angle and the distance between the UAV and the obstacle are considered.

References

Ali ZA and Zhangang H (2021) Multi-unmanned aerial vehicle swarm formation control using hybrid strategy. *Transactions of the Institute of Measurement and Control* 43(12): 2689–2701.

Cahyadi A, Darmawan E, Dewanto W, et al. (2020) Application of artificial potential field for coverage control with collision avoidance under sensing constraints. *Journal of Control, Automation and Electrical Systems* 31(2): 304–318.

Chang K, Ma D, Han X, et al. (2020) Lyapunov vector-based formation tracking control for unmanned aerial vehicles with obstacle/collision avoidance. *Transactions of the Institute of Measurement and Control* 42(5): 942–950.

Chen S, Yang Z, Liu Z, et al. (2018) An improved artificial potential field based path planning algorithm for unmanned aerial vehicle in dynamic environments. In: *2017 international conference on security, pattern analysis, and cybernetics*, Shenzhen, China, 15–17 December 2017, pp. 591–596. New York: IEEE.

Fu J, Wen G, Yu X, et al. (2020) Distributed formation navigation of constrained second-order multiagent systems with collision avoidance and connectivity maintenance. *IEEE Transactions on Cybernetics* 52: 2149–2162.

Haghighi H, Asadi D and Delahaye D (2021) Multi-objective cooperated path planning of multiple unmanned aerial vehicles based on revisit time. *Journal of Aerospace Information Systems* 18(12): 919–932.

Haghighi H, Sadati SH, Karimi J, et al. (2019) A hierarchical and prioritized framework in coordinated maneuver of multiple UAVs based on guidance regulator. *Journal of Aerospace Technology and Management* 11. Available at: https://www.scielo.br/j/jatm/a/B89H6F6CmtcPrxkYkYjJYqD/?lang=en

Hu J, Zhang H, Liu L, et al. (2020) Convergent multiagent formation control with collision avoidance. *IEEE Transactions on Robotics* 36(6): 1805–1818.

Huang S, Teo RSH and Tan KK (2019) Collision avoidance of multi unmanned aerial vehicles: A review. *Annual Reviews in Control* 48: 147–164.

Lee D, Jeong J, Kim YH, et al. (2018) An improved artificial potential field method with a new point of attractive force for a mobile robot. In: *2017 2nd international conference on robotics and automation engineering*, Shanghai, China, 29–31 December, pp. 63–67. New York: IEEE.

Li D, Pan Z and Deng H (2020) Two-dimensional obstacle avoidance control algorithm for snake-like robot in water based on immersed boundary-lattice Boltzmann method and improved artificial potential field method. *Transactions of the Institute of Measurement and Control* 42(10): 1840–1857.

Lin X, Wang ZQ and Chen XY (2020) Path planning with improved artificial potential field method based on decision tree. In: *27th*

Saint Petersburg international conference on integrated navigation systems, St. Petersburg, 25–27 May.

Lin Z, Yue M, Chen G, et al. (2021) Path planning of mobile robot with PSO-based APF and fuzzy-based DWA subject to moving obstacles. *Transactions of the Institute of Measurement and Control* 44: 121–132.

Liu R, Liu M and Liu Y (2019) Nonlinear optimal tracking control of spacecraft formation flying with collision avoidance. *Transactions of the Institute of Measurement and Control* 41(4): 889–899.

Mancini M, Bloise N, Capello E, et al. (2020) Sliding mode control techniques and artificial potential field for dynamic collision avoidance in Rendezvous Maneuvers. *IEEE Control Systems Letters* 4(2): 313–318.

Orozco-Rosas U, Montiel O and Seplveda R (2019) Mobile robot path planning using membrane evolutionary artificial potential field. *Applied Soft Computing Journal* 77: 236–251.

Pan Z, Zhang C, Xia Y, et al. (2022) An improved artificial potential field method for path planning and formation control of the multi-UAV systems. *IEEE Transactions on Circuits and Systems II: Express Briefs* 69: 1129–1133.

Park BS and Yoo SJ (2021) Connectivity-maintaining and collision-avoiding performance function approach for robust leader–follower formation control of multiple uncertain underactuated surface vessels. *Automatica* 127: 109501.

Qi J, Guo J, Wang M, et al. (2022) Formation tracking and obstacle avoidance for multiple quadrotors with static and dynamic obstacles. *IEEE Robotics and Automation Letters* 7(2): 1713–1720.

Raheem FA and Abdulkareem MI (2020) Development of A* algorithm for robot path planning based on modified probabilistic roadmap and artificial potential field. *Journal of Engineering Science and Technology* 15(5): 3034–3054.

Shevitz D and Paden B (1994) Lyapunov stability theory of nonsmooth systems. *IEEE Transactions on Automatic Control* 39(9): 1910–1914.

Singla A, Padakandla S and Bhatnagar S (2021) Memory-based deep reinforcement learning for obstacle avoidance in UAV with limited environment knowledge. *IEEE Transactions on Intelligent Transportation Systems* 22(1): 107–118.

Song J, Hao C and Su J (2020) Path planning for unmanned surface vehicle based on predictive artificial potential field. *International Journal of Advanced Robotic Systems* 17(2): 1–13.

Sui Z, Pu Z, Yi J, et al. (2021) Formation control with collision avoidance through deep reinforcement learning using model-guided demonstration. *IEEE Transactions on Neural Networks and Learning Systems* 32(6): 2358–2372.

Wang D, Wang P, Zhang X, et al. (2020) An obstacle avoidance strategy for the wave glider based on the improved artificial potential field and collision prediction model. *Ocean Engineering* 206: 107356.

Wu J, Luo C, Luo Y, et al. (2021) Distributed UAV swarm formation and collision avoidance strategies over fixed and switching topologies. *IEEE Transactions on Cybernetics*. Epub ahead of print 24 December. DOI: 10.1109/TCYB.2021.3132587.

Wu J, Wang H, Li N, et al. (2020) Formation obstacle avoidance: A fluid-based solution. *IEEE Systems Journal* 14(1): 1479–1490.

Yan T, Xu X, Li Z, et al. (2021) Fixed-time leader–following flocking and collision avoidance of multi-agent systems with unknown dynamics. *Transactions of the Institute of Measurement and Control* 43(12): 2734–2741.

Yang S, Bai W, Li T, et al. (2021) Neural-network-based formation control with collision, obstacle avoidance and connectivity maintenance for a class of second-order nonlinear multi-agent systems. *Neurocomputing* 439: 243–255.

Yun X and Tan KC (1997) Wall-following method for escaping local minima in potential field based motion planning. In: *International conference on advanced robotics*. *Proceedings*, Monterey, CA, 7–9 July, pp. 421–426. New York: IEEE.

Zappulla R, Park H, Virgili-Llop J, et al. (2019) Real-time autonomous spacecraft proximity maneuvers and docking using an adaptive artificial potential field approach. *IEEE Transactions on Control Systems Technology* 27(6): 2598–2605.